INSTITUTE OF PHYSICS PUBLISHING and INTERNATIONAL ATOMIC ENERGY AGENCY NUCLEAR FUSION

Nucl. Fusion **42** (2002) 1382–1392 PII: S0029-5515(02)55646-5

Fusion alpha parameters in tokamaks with high DT fusion rates

R.V. Budny

PPPL, Princeton University, PO Box 451, Princeton, NJ 08543, USA

E-mail: budny@princeton.edu

Received 4 March 2002, accepted for publication 21 October 2002
Published 27 November 2002
Online at stacks.iop.org/NF/42/1382

Abstract
Fusion alpha parameters are calculated for tokamaks with high DT fusion rates using the TRANSP plasma analysis code. Parameters include the fast alpha density n_α, fast alpha pressure normalized to magnetic field energy β_α, and its normalized gradient $-R \times \nabla(\beta_\alpha)$. The plasma conditions are taken from the plasmas in TFTR and JET with the highest DT fusion rates, and from plasmas in the proposed IGNITOR, FIRE, and ITER-FEAT tokamaks.

PACS numbers: 52.55.Fa, 52.55.Pi, 52.65.Pp

1. Introduction

For tokamaks to become practical sources of energy, large numbers of fusion ions must be confined long enough to heat the plasma. The interactions of fusion alphas on the plasma need to be understood to minimize detrimental effects and exploit beneficial effects. Examples of coupling of fast alphas to the thermal plasma that could be deleterious include stabilization of sawteeth [1, 2] and TAE activity [3].

The goal of this paper is to quantify fusion alpha parameters from a selection of proposed 'next step' tokamaks to facilitate future assessments of their effects. The first detailed Monte Carlo calculations for alpha effects in IGNITOR, FIRE, and ITER-FEAT are presented. Self-consistent models of the plasmas including their time evolutions are constructed using the TRANSP plasma analysis code (see [4] and references therein). Resulting profiles of alpha parameters, along with the $q_{\rm MHD}$ profiles and MHD equilibria are being used as inputs to codes such as the NOVA-K [5] and HINST [6, 7] for calculating TAE instability. These results are also of use for codes that calculate the MHD stability and micro-turbulence. Besides the summaries of the alpha parameters given here, electronic files of the MHD equilibria and of the phase space distributions of the fast ions are available.

Another use of these results is in designing experiments to study alpha parameters in burning plasmas. It is likely that auxiliary heating of some form will be used in the next step experiments, but if this generates fast ions (as can ICRH and NBI), these can mask or complicate the measurement of fast alpha effects. One possibility is to abruptly shut off the auxiliary heating in the burning plasma. If the auxiliary ions slow down faster than the alphas, there could be a window of opportunity.

Three proposed tokamaks are considered, IGNITOR [8–11], FIRE [12, 13], and ITER-FEAT [14]. One plasma from each is chosen for analysis. Ion cyclotron heating is assumed for each, with the ICRH frequency tuned to resonate with the first-harmonic of the He^3 ion-cyclotron frequency and the second-harmonic of T ions near the magnetic axis. In addition, negative ion neutral beam injection (NNBI) is assumed for ITER-FEAT to heat and drive plasma current.

Present-day experiments have produced modest powers from the DT fusion reaction. TFTR achieved 10.3 MW [15] and JET achieved 16.0 MW [16]. Identical analysis techniques are applied to these plasmas for comparing their achieved alpha parameters with those that can be expected from the three next step tokamaks. One advantage of using the same analysis tools for both present-day experiments and future experiments is that the definitions used for parameters such as triangularity are the same, minimizing the semantic ambiguities in extrapolating from present to future experiments.

2. Analysis techniques

2.1. TRANSP

The TRANSP plasma analysis code [4] is used to analyse the plasmas with the measured or assumed plasma parameters and to calculate the heat deposition profiles. TRANSP is a fixed-boundary code, so the plasma boundary is determined either by measurements in the TFTR and JET cases, or by assuming time evolutions of the major and minor radii, elongation, triangularity, and vertical displacement of the boundary in the cases of IGNITOR, FIRE, and ITER-FEAT. The MHD equilibria are calculated in TRANSP solving the Grad–Shafranov equation. The heat and particle fluxes are

 © 2002 IAEA, Vienna Printed in the UK

calculated from the continuity equations. The fusion ions (and beam ions when NBI is used) are treated using Monte Carlo methods [17] to model their source rates, neoclassical orbits, and slowing-down rates. There are various experimental confirmations of the accuracy of the TRANSP fast alpha calculations [18, 19].

The evolution of the q_{MHD} profile is calculated in TRANSP. To model effects of sawteeth, sawteeth crash times are assumed, and the TRANSP sawtooth model is used to helically mix the plasma current and fast ion profiles at the crash time if $q_{\mathrm{MHD}}(0) < 1.0$. Otherwise, poloidal field diffusion is calculated assuming neo-classical resistivity and bootstrap current [20], and driven currents in the case of NBI. The sawteeth simulations resulting from this analysis generally agree well with experimental observations in plasmas, such as L-mode, H-mode, and supershots with monotonic or mildly reversed q_{MHD} profiles. All five plasmas studied have conventional, monotonic q_{MHD} profiles, compared in figure 1 versus the toroidal flux variable, $x \equiv \sqrt{\text{normalized toroidal flux}}$, which is roughly equal to r/a. The profile for ITER-FEAT is affected by the assumed 1 MeV NNBI. If the sawtooth model is not invoked, the central values for q_{MHD} are predicted to evolve in time to $\approx$0.7 in IGNITOR and ITER-FEAT. Alternative start-up evolutions can keep $q_{\mathrm{MHD}} > 1.0$. For the plasma start-up assumed for FIRE, $q_{\mathrm{MHD}}(0)$ remains above unity for most of the auxiliary heating phase. The values of q_{MHD} at the edge, designated $x = 1$, are at the $x = 0.98$ flux surface. Basic plasma conditions during an approximately steady-state phase of each plasma are summarized in table 1.

The power radiated by the plasmas is simulated by TRANSP, assuming coronal equilibrium, similar to the techniques in [21]. The power is separated into bremsstrahlung, line, and cyclotron radiation. The bremsstrahlung and line radiation emission powers are computed using tabulated rate coefficients. The cyclotron radiation power emission is calculated by a simple formula given in [22]. The predictions for a selected time with approximately steady-state conditions are given in table 2. In the cases of the TFTR and JET plasmas the measured radiation power emissions are larger than the predictions, and the measured rates are used in the power balance calculations.

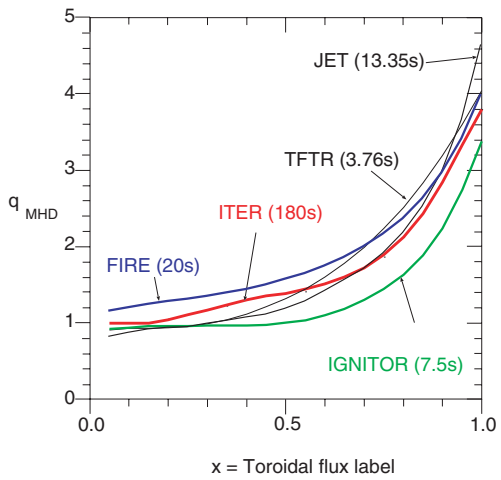

Figure 1. Profiles of q_{MHD} in the TFTR, JET, IGNITOR, FIRE, and ITER plasmas during the steady-state phases.

The ICRH power deposition profiles are computed using the SPRUCE full wave, reduced-order package [23] in TRANSP. For the next step tokamaks, relatively close-fitting antenna are assumed, with a strap separation $\Delta = 30$ cm. The relative phasing of the straps are assumed to be π. The $k_{\|}$ spectra are assumed to have two values at $\pm\pi/\Delta$.

One parameter of special interest is the minority 'tail temperature', defined by

$$T_{\mathrm{min}} = \left(\frac{2}{3}\right)\frac{W_{\mathrm{min},\perp}}{n_{\mathrm{min}}}, \tag{1}$$

where $W_{\mathrm{min},\perp}$ is the energy density of the RF-resonant ion species in the plane perpendicular to the magnetic field and n_{min} is the density of that ion species. The predicted values of $T_{\mathrm{min}}(0)$ are low, comparable to $T_{\mathrm{i}}(0)$ in FIRE and ITER-FEAT. The results are summarized in table 3.

The accumulation of alpha ash in the next-step tokamaks is simulated assuming

$$\Gamma_{\mathrm{ash}} = (-D_{\mathrm{ash}}\nabla n_{\mathrm{ash}} + V_{\mathrm{ash}} n_{\mathrm{ash}})A_{\mathrm{surf}}, \tag{2}$$

where A_{surf} is the area of the flux surface at x. The value of D_{ash} is assumed to be constant, and the value of V_{ash} is assumed to be zero, excluding the pessimistic possibility of an inward pinch velocity. The ash density, n_{ash}, is calculated from the local source rate of thermalized fusion alphas and recycling influx from the wall.

The recycling coefficient of the ash, R_{ash}, defined as the ratio of the fluxes entering and exiting the plasma boundary, $\Gamma_{\mathrm{in}}(1)/\Gamma_{\mathrm{out}}(1)$ is assumed (optimistically) to be low, 20%, corresponding to good pumping of the ash. Under these assumptions, the ash accumulation in the plasmas does not reduce the simulated DT fusion yield significantly in any of the burning plasmas studied. The ash confinement time is defined by the ratio $(\int n_{\mathrm{ash}}\,\mathrm{d}V)/\Gamma_{\mathrm{ash}}$. Generally the effective confinement time is defined as

$$\tau^{*}_{\mathrm{ash}} = \frac{\tau_{\mathrm{ash}}}{1 - R_{\mathrm{ash}}}. \tag{3}$$

Results are summarized in table 4.

The thermal energy confinement and anomalous heat transport coefficients are computed by TRANSP. The energy confinement is calculated from

$$\tau_{E,\mathrm{th}} = \frac{W_{\mathrm{th}}}{P_{\mathrm{loss}}} \tag{4}$$

with $P_{\mathrm{loss}} = P_{\mathrm{i,cond}} + P_{\mathrm{e,cond}} + P_{\mathrm{i,conv}} + P_{\mathrm{e,conv}} + P_{\mathrm{rad}} + P_{\mathrm{cx}} = P_{\mathrm{heat}} - \mathrm{d}W_{\mathrm{th}}/\mathrm{d}t - P_{\mathrm{misc}}$, where P_{heat} is the heating power of the thermal plasma and P_{misc} is the heating power that does not couple to the thermal plasma, such as orbit and ripple losses. Results are summarized in table 5.

2.2. *Empirical energy confinement scaling laws*

The next step plasmas are very different from present-day plasmas in many ways, but comparisons of their performance with empirical scaling laws could be useful for assessing the likelihood of being able to produce the plasmas. Several

Table 1. Summary of boundary and plasma parameters at a steady-state time. Most of the parameters are inputs. Exceptions are the Shafranov shift of the magnetic axis $R_{\rm Shaf}(0)$, $I_{\rm boot}$ (calculated using the NCLASS code [20]), $B_{\rm Pol}$, $I_{\rm beam}$ and $q_{\rm MHD}$ (calculated accounting for poloidal field diffusion). The time-evolving geometry of the boundary ($x = 1$) is specified. $A_{\rm imp}$ and $Z_{\rm imp}$ are chosen as the atomic mass and charge of an effective impurity ion whose density profiles are determined by the assumed (or in the cases of TFTR and JET measured) $Z_{\rm eff}$ profiles after the computed helium ash contribution is subtracted.

Tokamak	TFTR	JET	IGNITOR	FIRE	ITER
RUNID	80539A24	42976C10	30000B22	50000A26	03000A24
Steady-state time [s]	3.76	13.35	6.5	20.0	180.0
R(1) [m]	2.52	2.92	1.32	2.14	6.2
$R_{\rm Shaf}(0)$ [cm]	17.5	8.0	2.7	3.2	15.4
$a(1)$ [m]	0.87	0.94	0.48	0.60	2.0
$\kappa(1)$	1.02	1.80	1.80	2.00	1.85
$\delta(1)$	0.02	0.35	0.40	0.49	0.50
$P_{\rm vol}(1)$ [m^3]	38.8	84.0	9.9	27.2	820
$B_{\rm Tor}$ [T]	5.5	3.5	13.0	10.0	5.3
$B_{\rm Pol}(1)$ [T]	0.6	0.5	2.5	1.35	0.85
$I_{\rm p}$ [MA]	2.7	4.0	11.0	7.7	15.0
$I_{\rm beam}$ [MA]	0.05	0.18	N/A	N/A	1.2
$I_{\rm boot}$ [MA]	0.65	0.40	1.0	1.8	3.0
$q_{\rm MHD}(1)$	4.05	4.7	3.6	4.0	3.8
$T_{\rm e}(0)$ [keV]	13.2	11.0	9.9	11.9	23.5
$\langle T_{\rm e}\rangle$ [keV]	8.7	7.3	5.2	7.2	10.0
$T_{\rm i}(0)$ [keV]	41.0	23.0	9.9	11.9	19.5
$\langle T_{\rm i}\rangle$ [keV]	8.7	7.3	5.2	7.2	8.6
$A_{\rm h}$	2.20	2.53	2.5	2.5	2.5
$n_{\rm e}(0)$ [10^{20} m^{-3}]	1.02	0.45	9.4	4.9	1.02
$\bar{n}_{\rm e}$ [10^{20} m^{-3}]	0.51	0.46	5.3	4.0	1.00
$\langle n_{\rm e}\rangle$ [10^{20} m^{-3}]	0.40	0.48	3.3	3.4	0.98
$\bar{n}_{\rm e}/\bar{n}_{\rm GW}$	0.46	0.32	0.35	0.59	0.84
$A_{\rm imp}$	12.4	12.0	12.0	8.0	8.0
$Z_{\rm imp}$	6.2	6.0	6.0	4.0	4.0
$Z_{\rm eff}(0)$	3.1	1.5	1.2	1.39	1.54
$n_{\rm imp}(0)/n_{\rm e}(0)$ (%)	5.5	1.5	0.5	2.7	3.9

Table 2. Heating and heat loss rates at the steady-state times used in table 1. $P_{\rm ext}$ is the sum of the applied Ohmic, NBI, and ICRH (when applicable) heating powers. $P_{\rm heat}$ is the total heating power of the thermal plasma calculated by TRANSP. The conduction and convection losses are given at the $x = 0.9$ surface since they vary only weakly near that surface, but rapidly at larger radii. The $P_{\rm brem}$, and $P_{\rm line}$ contributions to $P_{\rm rad}$ are computed in TRANSP using a coronal equilibrium model. The $P_{\rm cyc}$ contribution to $P_{\rm rad}$ is computed using a simple estimate. The values for $P_{\rm rad}$ measured in TFTR and JET are considerably higher than the sum $P_{\rm brem} + P_{\rm line} + P_{\rm cyc}$. Several explanations could account for this: (1) these plasmas are not in coronal equilibria; (2) non-negligible amounts of high Z impurities are contributing; or (3) the bolometry measurements of $P_{\rm rad}$ are wrong (for instance, they could be measuring charge-exchange particles as well as photons).

Tokamak	TFTR	JET	IGNITOR	FIRE	ITER
RUNID	80539A24	42976C10	30000B22	50000A26	03000A24
Steady-state time [s]	3.76	13.35	6.5	20.0	180.0
$P_{\rm Ohmic}$ [MW]	0.5	0.4	6.0	1.3	1.1
$P_{\rm NB}$ [MW]	39.5	22.4	0.0	0.0	33.0
$P_{\rm RF}$ [MW]	0.0	3.2	24.0	11.2	Early
$P_{\rm ext}$ [MW]	40.0	26.0	30.0	12.5	34.1
$P_{\rm DT}$ [MW]	9.5	15.7	75.1	149	404
$P_{\alpha\text{-el}}$ [MW]	1.1	2.1	12.4	24.0	57
$P_{\alpha\text{-ion}}$ [MW]	0.1	0.3	2.6	5.6	22
P_{α} [MW]	1.2	2.4	15.0	29.6	80
$P_{\rm ext} + P_{\alpha}$ [MW]	41.2	28.4	45.0	42.0	114
$P_{\rm heat}$ [MW]	27.0	16.4	44.6	42.1	114
$P_{\rm i,cond}(0.9)$ [MW]	11.0	10.1	19.0	13.2	90.0
$P_{\rm i,conv}(0.9)$ [MW]	2.0	7.5	0.1	0.6	0.9
$P_{\rm e,cond}(0.9)$ [MW]	7.0	0.0	20.5	19.0	3.0
$P_{\rm e,conv}(0.9)$ [MW]	0.0	1.0	0.1	0.5	0.4
$P_{\rm brem}$ [MW]	0.3	0.6	3.4	8.2	21.0
$P_{\rm line}$ [MW]	0.1	0.1	0.4	0.1	4.0
$P_{\rm cyc}$ [MW]	0.1	0.1	0.1	0.02	0.6
$P_{\rm rad}$ [MW]	3.2	3.3	4.1	9.0	26.0
$P_{\rm cx}$ [MW]	0.5	9.2	0.1	2.0	0.8

Table 3. Summary of ICRH parameters. The ICRH frequencies Ω_{RF}, powers P_{RF}, and minority ion profiles, n_{min} are assumed. The computed RF minority tail temperature T_{min} is defined in equation (1). The fractions of the heating power transferred directly to the minority ion and to the plasma species are calculated in TRANSP using SPRUCE [23]. The transfer of energy from the fast minority ions to the thermal plasma is calculated by TRANSP. For IGNITOR with ICRH at both 120 and 140 GHz, the heating fractions of each are given. Very small concentrations of certain impurities could cause resonances and power absorption far from the magnetic axis and change the power fractions. For instance, with the assumed Ω_{RF} and B_{Tor} for ITER, very small amounts of boron could resonate near the outer edge, absorbing much of P_{RF}.

Tokamak	JET	IGNITOR	FIRE	ITER
RUNID	42976C10	30000B23	50000A28	03000A24
Time [s]	13.35	6.5	20.0	140.0
Ω_{RF} [MHz]	51.2–56.5	120/140	100	53
P_{RF} [MW]	3.4	12/12	11	20
Minority ion	H	He^3	He^3	He^3
n_{min}/n_e (%)	2.0	2.0	2.0	3.0
$T_{min}(0)$ [keV]	150	≈130	10.0	28.0
$P_{RF\text{-}min}/P_{RF}$ (%)	60	61/47	62	45
$P_{RF\text{-}T}/P_{RF}$ (%)	1	11/14	10	4
$P_{RF\text{-}D}/P_{RF}$ (%)	17	6/11	2	3
$P_{RF\text{-}\alpha}/P_{RF}$ (%)	0	0/3	1	0
$P_{RF\text{-}e}/P_{RF}$ (%)	13	22/23	24	48

Table 4. Summary of alpha ash parameters. The diffusivity of the He ash D_{ash} and the recycling coefficient at the boundary R_{ash} are assumed. The time evolutions of the profiles of the confinement time defined in equation (3) and the ash density are calculated by TRANSP. These are in steady state for the FIRE and ITER plasmas.

Tokamak	IGNITOR	FIRE	ITER
RUNID	30000B22	50000A26	03000A24
Time [s]	6.5	20.0	180.0
R_{ash} (%)	20	20	20
D_{ash} [$m^2\,s^{-1}$]	0.1	0.1	0.8
$\tau_{ash}(0.95)$ [s]	23.0	1.25	1.55
$n_{ash}(0)/n_e(0)$ (%)	0.9	1.2	0.7

empirical scaling laws for the thermal energy confinement time give accurate fits to existing data. One such fit for ELMy H-mode plasmas [24] is

$$\tau_{IPB98(y,2)} = 0.144 I_p^{0.93} R^{1.39} a^{0.58} \bar{n}_e^{0.41} B_{Tor}^{0.15} A_h^{0.19} \kappa^{0.78} P^{-0.69}, \quad (5)$$

where I_p is the plasma current [MA], $\bar{n}_e$ is the line-averaged electron density [$10^{20}\,m^{-3}$], B_{Tor} is the toroidal magnetic field [T], A_h is the volume-averaged isotopic mass of the hydrogenic species, and P, the total heating power [MW] ($=P_{aux} + P_{Ohmic} + P_\alpha$). In the following P_{heat} is used for P, which is lower for the TFTR and JET plasmas which have non-negligible losses of fast ions (shine-through, orbits intercepting objects, stochastic toroidal field ripple, charge-exchange). Thus, the definition of $\tau_{ITB98(y,2)}$ used here is slightly higher than the usual definition.

Although the fit $\tau_{IPB98(y,2)}$ is not applicable to TFTR supershots or to the JET hot-ion H-mode plasma, it agrees surprisingly well with $\tau_{E,th}$, as seen in table 5. The fit is more relevant for comparison with the values calculated for the ELMy H-mode plasmas assumed for FIRE and ITER-FEAT plasmas. The estimate of energy confinement time given by the ratio of the total stored energy and the heating power is higher than $\tau_{E,th}$, due to the fast ion contributions to the total energy.

There are other features of ELMy H-mode plasmas that affect their energy confinement. They tend to have higher energy confinement when the triangularity of their boundary, $\delta(1)$, is large, and when their electron density profile is more peaked. They tend to have lower confinement when $\bar{n}_e$ is high (or very low) relative to the Greenwald density defined as $n_{GW} = I_p/(\pi a^2)$ [$MA\,m^{-2}$]. An empirical correction factor that accounts for these effects is given in [25]:

$$f = 0.71 + 0.33\delta(1) - 1.58(f_{GW} - 0.63)^2 + 0.58\left(\frac{\bar{n}_e}{n_{ped}} - 1\right), \quad (6)$$

where $f_{GW} = \bar{n}_e/n_{GW}$ and n_{ped} is the electron density at the top of the pedestal. The corrected fit for the confinement time is the product $f\tau_{IPB98(y,2)}$.

Another parameter listed in table 5 is the L-mode [24] fit to τ_E for L-mode plasmas:

$$\tau_L = 0.0578 I_p^{0.96} R^{1.89} a^{-0.06} \bar{n}_e^{0.40} B_{Tor}^{0.03} A_h^{0.20} \kappa^{0.64} P^{-0.73}. \quad (7)$$

Table 5 shows that τ_L is about $\tau_{IPB(y,2)}/2$ for the plasmas considered.

3. Plasma and alpha parameters

3.1. TFTR

The TFTR plasma chosen was a supershot [15] obtained with extensive wall conditioning and injection of Li pellets into the Ohmic phase to reduce the influx of hydrogenic and impurity ions. The auxiliary heating consisted of 25.3 MW of T-NBI, 14.2 MW of D-NBI, and 0.5 MW Ohmic heating. The plasma experienced a minor disruption late in the flat-top, followed by a carbon bloom, probably caused by a flake or limiter dust entering the plasma. This event caused the total number of electrons in the plasma to increase by a factor of 2.6 in 200 ms, increasing f_{GW} from 0.46 to nearly 1.0, while broadening the density profile considerably. With the decreased slowing down time, the alpha heating power increased about 30% during the bloom, and $\max\{P_\alpha/P_{heat}\}$ increased by a factor of three. Due to the need for steady-state conditions in a reactor, the parameter values are quoted in tables 1–5, just before the minor disruption and bloom.

Profiles of the plasma parameters in TFTR before the bloom are shown in figure 2. The profile for the anomalous heat conduction, χ_{eff}, rises steeply from the core to the edge, and is near 1.5 [$m^2\,s^{-1}$] at the mid-radius ($x = 0.5$). Time evolutions of selected plasma parameters are shown in figure 3. Table 5 gives a summary of some parameters of use for quantifying effects of alpha particles such as the slowing down time (for energy to slow to $1.5T_i$) in the centre.

3.2. JET

The JET plasma chosen was a hot-ion H-mode [16] achieved by starting with a relatively low-density Ohmically heated plasma. The auxiliary heating consisted of 11.9 MW D-NBI,

Table 5. Examples of calculated plasma parameters at the steady-state times used in tables 1 and 2. Here $\beta_{\rm Pol}$ is defined as $\langle p\rangle/(\langle B^2_{\rm Pol}\rangle/(8\pi))$ where $\langle p\rangle$ is the volume-averaged total equilibrium pressure and $\langle B^2_{\rm Pol}\rangle$ is the differential volume average of the poloidal field squared, over the outermost flux surface. The maximum value for $P_\alpha/P_{\rm heat}$ occurs at the magnetic axis for all but FIRE. The maximum value for $-R\times\nabla(\beta_\alpha)$ occurs around $x = 0.20$–0.40, as shown in figure 18.

Tokamak	TFTR	JET	IGNITOR	FIRE	ITER
RUNID	80539A24	42976C10	30000B22	50000A26	03000A24
Steady-state time [s]	3.76	13.35	6.5	20.0	180.0
$\langle\beta_{\rm total}\rangle$ (%)	1.03	2.17	1.10	2.10	2.55
$\beta_{\rm total}(0)$ (%)	6.0	4.9	4.7	4.6	6.5
$\langle\beta_{\rm thermal}\rangle$ (%)	0.60	1.79	1.05	2.02	2.41
$\beta_{\rm Pol}$	0.51	0.94	0.24	0.95	0.85
$\beta_{\rm n}$	1.85	1.95	0.62	1.64	1.85
$W_{\rm tot}$ [MJ]	7.5	17.0	11.4	35.0	360
$W_{\rm tot}/(P_\alpha+P_{\rm ext})$ [s]	0.18	0.61	0.25	0.83	3.16
$\tau_{E,\rm th}$ [s]	0.13	0.59	0.25	0.80	2.98
$\tau_{\rm IPB98(y,2)}$ [s]	0.14	0.55	0.51	0.80	3.15
$\tau_{\rm L}$ [s]	0.066	0.30	0.23	0.41	1.40
$\tau_{\rm slow}(0)$ [s]	0.48	1.0	0.042	0.097	0.85
$\tau_{\rm scat}(0)$ [s]	5.8	21	1.5	2.5	10.8
$P_\alpha(0)$ [MW m^{-3}]	0.28	0.08	13.0	5.0	0.55
$\max\{P_\alpha/P_{\rm heat}\}$	0.20	0.23	0.65	0.76	0.98
$n_{\rm beam}(0.4)/n_{\rm e}(0.4)$ (%)	32.0	8.0	N/A	N/A	0.40
$n_\alpha(0)/n_{\rm e}(0)$ (%)	0.17	0.28	0.13	0.19	0.85
$\beta_\alpha(0)$ (%)	0.30	0.4	0.23	0.30	1.20
$\langle\beta_\alpha\rangle$ (%)	0.034	0.1	0.031	0.030	1.30
$\max\{-R\times\nabla(\beta_\alpha)\}$ (%)	2.0	2.3	0.9	1.4	3.8
$v_\alpha(0)/v_{\rm Alfven}(0)$	1.72	1.52	2.10	2.10	1.86

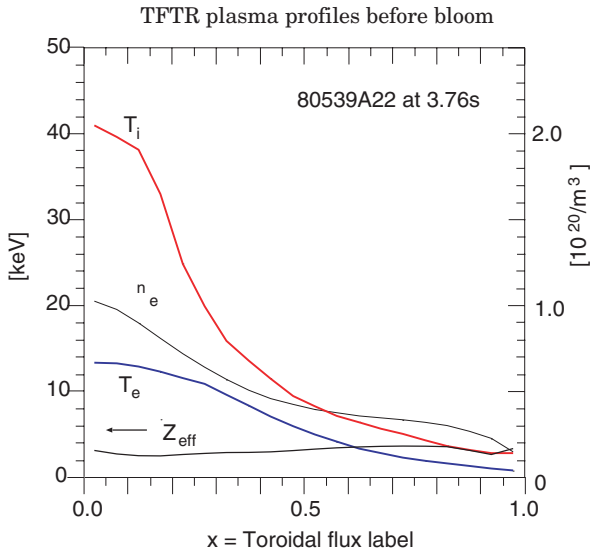

Figure 2. Profiles of the TFTR supershot before the carbon bloom.

10.5 MW T-NBI, 0.4 MW Ohmic, and 3.2 MW ICRH tuned to resonate with hydrogen-minority ions near the plasma axis. The plasma energy increased throughout an ELM-free period lasting 0.9 s. Then, a series of three giant ELMs occurred. The values of the alpha parameters quoted in table 5 are at 13.35 s, just before the first giant ELM, and the end of the charge-exchange spectroscopy data. Higher values are recorded [26] 100 ms after the first giant ELM; however, the giant ELMs do not appear compatible with practical reactors.

The results of the ICRH modelling are summarized in table 3. The profiles of the plasma parameters just before the first giant ELM are shown in figure 4. The profile for $\chi_{\rm eff}$ is relatively flatter than that for the TFTR supershot, and is near 0.4 [m^2 s^{-1}] at the mid-radius. The time evolutions of some of the plasma parameters are shown in figure 5.

3.3. IGNITOR

IGNITOR [8–11] is designed to have a high toroidal field with normal conducting magnets, so the plasma durations will be relatively short. A web site for IGNITOR is http://www.frascati.enea.it/ignitor/. IGNITOR is not designed to have a divertor, so the plasma boundary will be shaped by limiters. High plasma current and high electron density with a peaked profile are assumed. Some of the plasma parameters differ slightly from those given in [7–11]. Profiles during the flat-top are shown in figure 6. The limiters are designed to be made of molybdenum, but the dominant impurity species is assumed to be carbon with the $Z_{\rm eff}$ profile shown in figure 6. The alpha ash density is also shown. The discharge duration is too short for the alpha ash to obtain steady state. Even if $R_{\rm ash}$ were unity, the accumulation of ash would not reduce $P_{\rm DT}$ significantly.

Although Ohmic ignition is envisioned, the case considered here has 24 MW of He^3-minority ICRH. Two frequencies are assumed, 12 MW at 120 MHz and 12 MW at 140 MHz to place one of the resonances near the magnetic axis both during the ramp-up of the toroidal field, and the flat-top. A contour plot of the power deposition is shown in figure 7. The value computed for $\tau_{E,\rm th}$ is nearly equal to the L-mode fit, $\tau_{\rm L}$, and below the ELMy H-mode fit $\tau_{\rm IPB98(y,2)}$. Thus, the assumed profiles and heating do not reflect the possibility of a dramatic enhancement of confinement that could result from assumed high values for $n_{\rm e}(0)$ and peakedness.

The assumed time evolutions for the plasma parameters are shown in figure 8. The density and temperature profiles

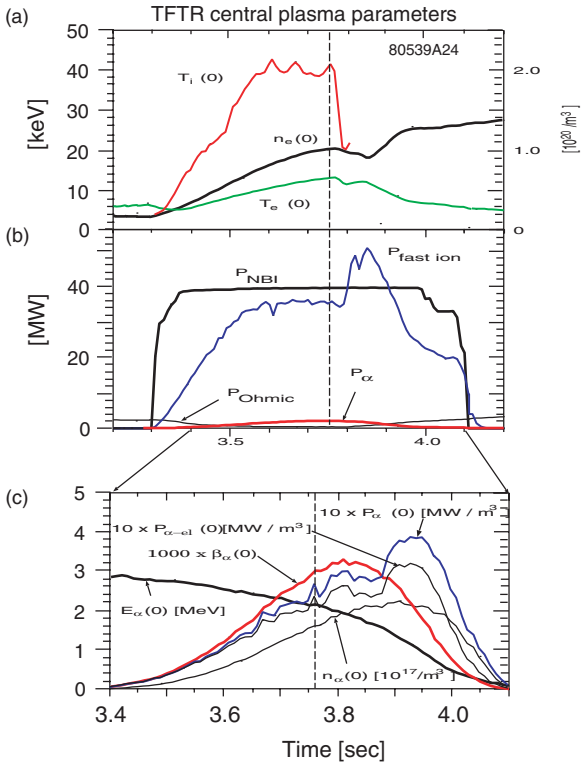

Figure 3. Time evolution of parameters in the TFTR supershot. (*a*) The charge-exchange-measured T_i profile (for carbon) became hollow with unrealistically low central values after the density became too high for good beam penetration. (*b*) $P_{\text{fast ion}}$ is the heating power of the thermal plasma from the NBI and alphas. (*c*) E_α is the average energy of the fast alphas in the core. The alpha parameters in (*c*) are volume-averaged out to the $x = 0.1$ flux surface to reduce Monte Carlo fluctuations. The vertical dashed lines indicate the time of the profiles in figure 2 (3.76 s).

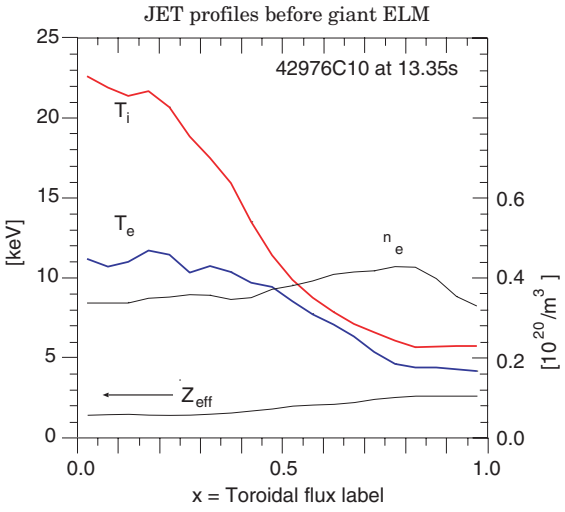

Figure 4. Profiles of the JET hot-ion H-mode plasma before the series of giant ELMs.

are assumed to ramp up slowly in the Ohmic phase, and then rapidly as the ICRH and alpha heating increase in order to keep high (conservative) values for χ_i and χ_e. In contrast, the density and temperature profiles are assumed to ramp up in a more steady rate in many of the IGNITOR publications.

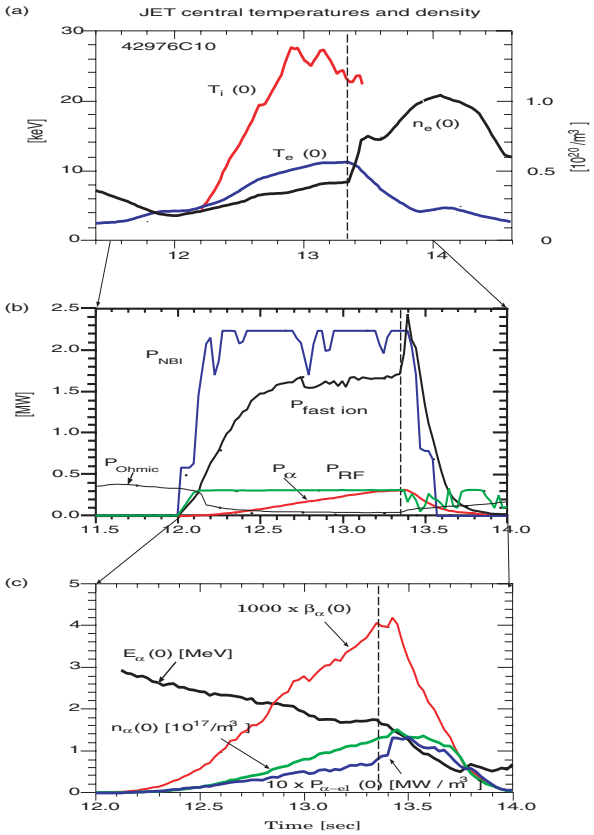

Figure 5. Time evolution of parameters in the JET plasma. The vertical dashed lines indicate the time of the profiles in figure 4 (14.35 s).

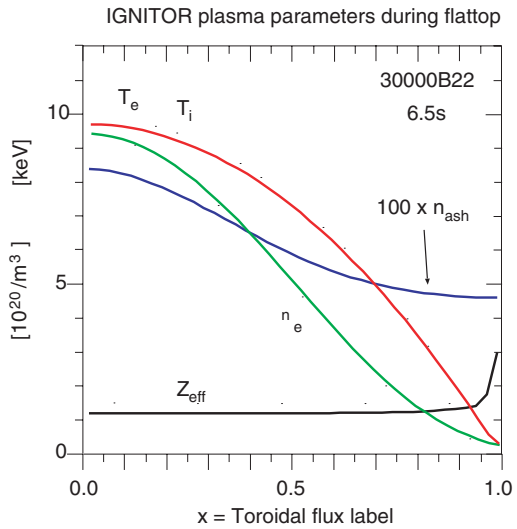

Figure 6. Profiles of the IGNITOR plasma in the flat-top phase. The He^4 ash density times 100 is computed from the fast alpha thermalization assuming $R_{\text{ash}} = 20\%$ and $D_{\text{ash}} = 0.1\,[\text{m}^2\,\text{s}^{-1}]$.

The assumed start-up has little effect on the calculated fusion parameters that are the focus of this paper. Note that the plasma reaches a steady state so the $\mathrm{d}W/\mathrm{d}t$ term has a negligible effect in the calculated $\tau_{E,\text{th}}$. The computed value for χ_{eff} is $\approx 0.8\,[\text{m}^2\,\text{s}^{-1}]$ near the mid-radius, and higher elsewhere, i.e. less demanding of transport reduction.

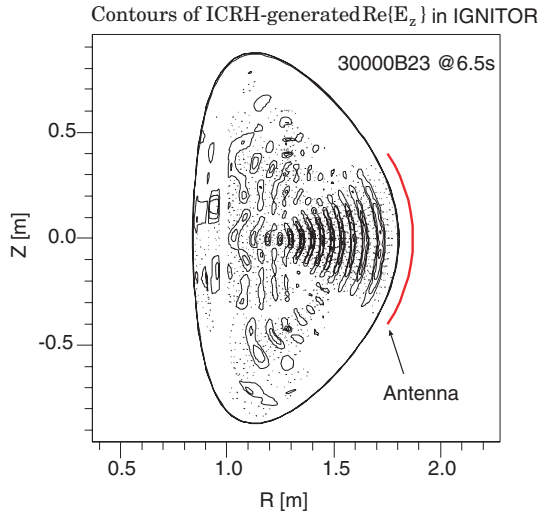

Figure 7. Contours of the 120 MHz ICRH-induced Re$\{E_r\}$ in the IGNITOR plasma.

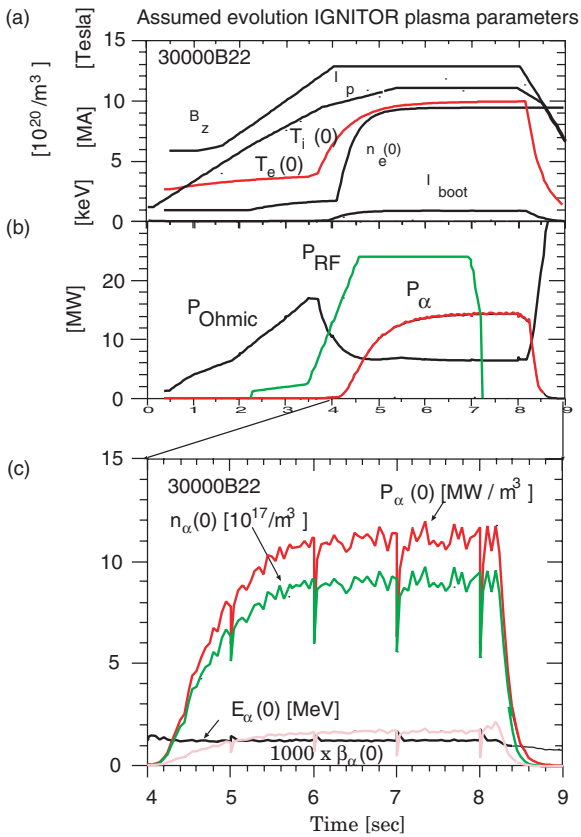

Figure 8. Time evolution of parameters in the IGNITOR plasma.

To get the same thermal plasma conditions (and alpha parameters) without the additional 24 MW of ICRH the minimum value of $\chi_{\rm eff}$ must be about 0.3 [m^2 s^{-1}], i.e. more optimistic. The value of $\tau_{E,\rm th}$ would need to be twice the value in table 5, about 0.53 [s]. This is still considerably lower than the value of $\tau_{\rm IPB98(y,2)} = 0.85$ s.

The TRANSP sawtooth mixing model is used to helically mix the current and fast ions at a sawtooth period of 1 s. This clamps $q_{\rm MHD}(0)$ to remain near 1.0. With the plasma start-up

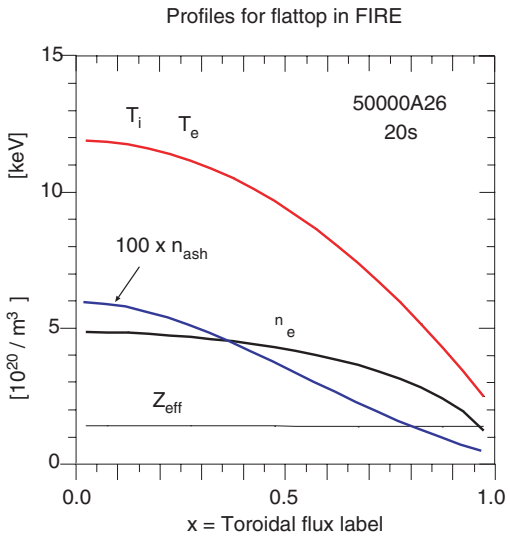

Figure 9. Profiles of the FIRE plasma in the flat-top phase. The He^4 ash density times 100 is computed from the fast alpha thermalization assuming $R_{\rm ash} = 20\%$ and $D_{\rm ash} = 0.1$ [m^2 s^{-1}], and is in steady state at the time shown.

assumed here, the central $q_{\rm MHD}$ would evolve down to 0.7 if the sawtooth model were turned off. The sawtooth mixing of the fast alpha particles reduces the alpha parameters in the centre, as seen in figure 8(c). Even though the mixing radius is relatively large, the central alpha heating and alpha density recover very rapidly. Sawteeth reductions of the central plasma densities and temperatures are not modelled here.

3.4. FIRE

FIRE [12, 13] is designed to have normal conducting magnets, and a double-null divertor geometry. A web site for FIRE is http://fire.pppl.gov. The plasma is assumed to operate in the standard ELMy H-mode regime. Profiles of the plasma parameters are shown in figure 9. These are based on predictions from the TSC code [27].

Since the divertors are designed to be coated with beryllium, the dominant impurity species, besides the He ash, is assumed to be Be with the $Z_{\rm eff}$ profile shown in the figure. Accumulation of alpha ash is modelled assuming the ash has an anomalous diffusivity of 0.1 m^2 s^{-1} with no pinch term. With the computed alpha thermalization rate and wall recycling rate (20%), the ash accumulates to the steady-state profile shown in figure 9, which has little impact on the fusion rate. If $R_{\rm ash}$ were unity, the predicted $P_{\rm DT}$ would decrease 13% from the peak rate within 12 s. Aggressive pumping may be needed to keep the ash recycling low. The confinement time of the ash is computed to be 1.2 s near the plasma boundary.

The plasma is heated with ICRH at a frequency of 100 MHz to resonate with He^3 on-axis. The $P_{\rm RF}$ is 20 MW early, and lowered to 11 MW as the alpha heating increases, to keep $P_\alpha + P_{\rm ext}$ roughly constant. A contour plot of the power deposition and antenna position is shown in figure 10.

The computed value for $\tau_{{\rm th},E}$ equals $\tau_{\rm IPB98(y,2)}$, but the enhancement factor given in equation (6) would increase $\tau_{\rm IPB98(y,2)}$ by a factor of 1.6. The computed value for $\chi_{\rm eff}$ is near 0.34 [m^2 s^{-1}] near $x = 0.8$, and higher elsewhere. The

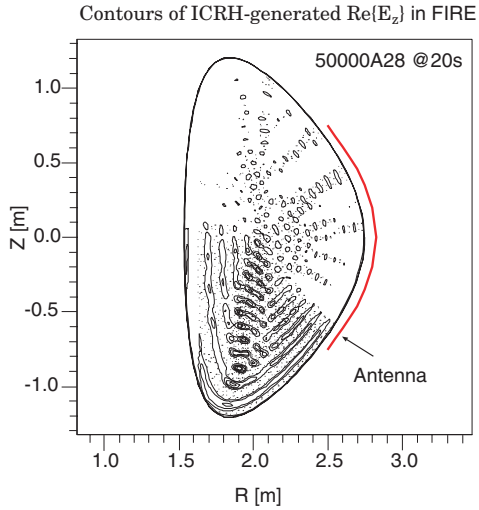

Figure 10. Contours of ICRH-induced Re$\{E_r\}$ in the FIRE plasma.

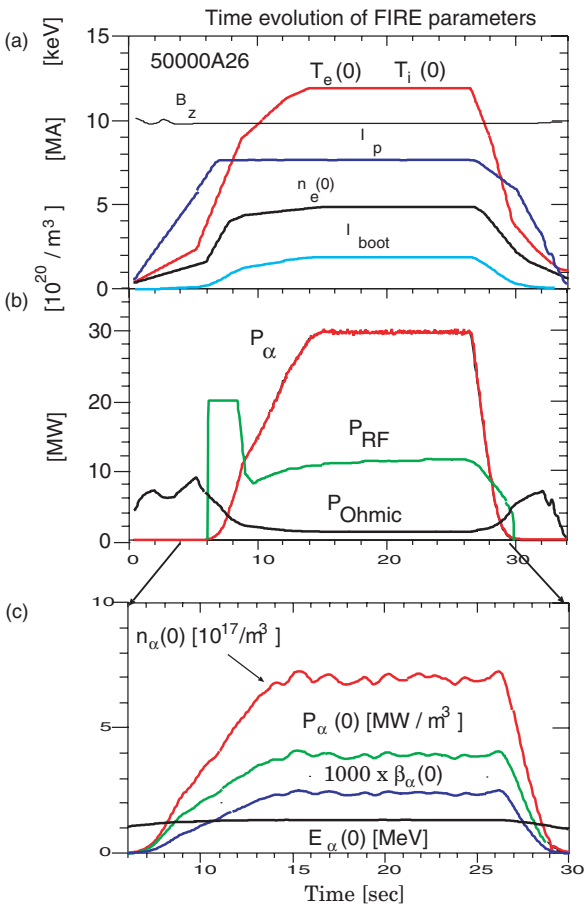

Figure 11. Time evolution of parameters in the FIRE plasma. P_{RF} is made high early to obtain the L–H mode transition, and is then reduced.

assumed time evolutions of plasma parameters are shown in figure 11.

3.5. ITER-FEAT

ITER-FEAT [14] is designed to have superconducting magnets for long pulse duration, and a single-null divertor geometry.

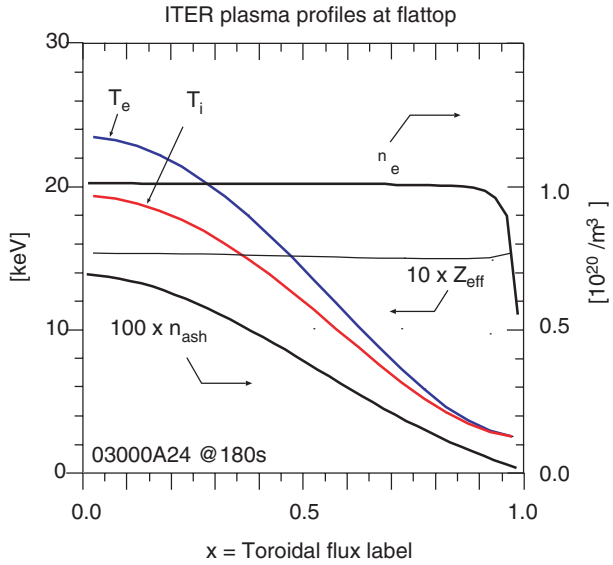

Figure 12. Profiles of the ITER plasma. The He^4 ash density times 100 is computed from the fast alpha thermalization assuming $R_{ash} = 20\%$ and $D_{ash} = 0.8\,[m^2\,s^{-1}]$, and is in steady state at the time shown.

A web site for ITER is http://www.itereu.de. The plasma is assumed to be in the ELMy H-mode regime with profiles close to those in [14] with a target DT fusion yield of $P_{DT} = 400$ [MW]. Profiles of the plasma parameters are shown in figure 12. The profile of T_e in [14] is about 20% higher than that of T_i. TRANSP computes the thermal ion heating at 180 s to be 38 [MW] and the thermal electron heating to be 76 [MW]. Their total is given in table 2. The density is sufficiently high that the electron–ion energy transfer rate is 51 [MW]. Thus the computed χ_e is low compared to χ_i, especially at large radii. This is reflected in $P_{i,cond}(0.9) \gg P_{e,cond}(0.9)$ in table 2.

Accumulation of alpha ash is modelled assuming the ash has an anomalous diffusivity of 0.8 $m^2\,s^{-1}$ with no pinch. With the computed alpha thermalization rate and wall recycling rate (20%), the ash accumulates to the steady-state profile shown in figure 12, which has little impact of depletion on the fusion rate. The confinement time of the ash near the plasma boundary is computed to be 1.6 s.

The boundary of the plasma is grown from circular to an up/down asymmetric shape, shown in figure 13. The assumed ICRH antenna position and computed contours of the induced E_z are shown in figure 14. Time evolutions of plasma parameters are shown in figure 15. The sawtooth period is assumed to be 10 s.

The external heating is assumed to consist of 20 MW of ICRH staggered with 33 MW of NNBI. This staggering allows the study of the heat fluxes and fast ion parameters in three cases with the same assumed plasma profiles: RF-only, RF + NB, and NB-only. The NNBI is assumed to consist of 1 MeV (D) neutrals from a negative ion-beam system injected in the co-plasma current direction, at a tangency radius of 6 m. This generates a beam-driven current profile that is broad with a total driven current of 1.2 MA. The bootstrap current profile is large near the edge. The effects of these currents on the q_{MHD} profile were shown in figure 1.

During the NNBI the ratio of the beam and fast alpha density is near unity in the centre and increases to 20 near

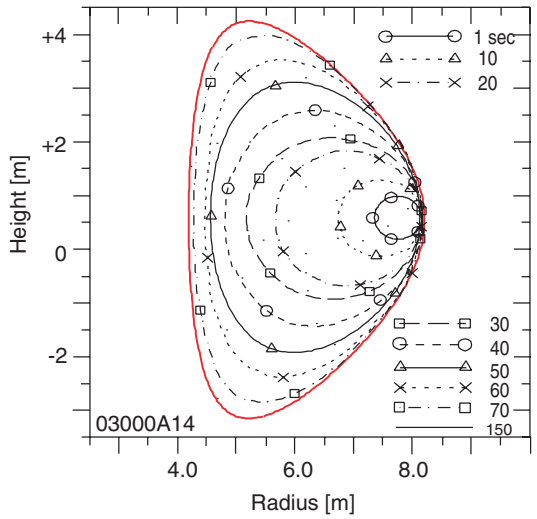

Figure 13. Assumed boundary for the ITER plasma.

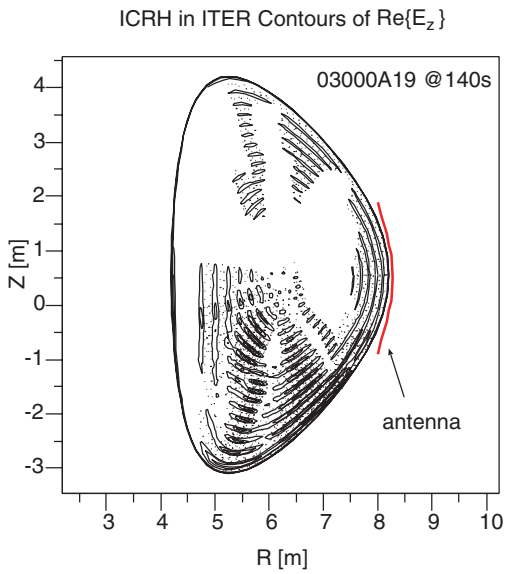

Figure 14. Contours of the ICRH-induced Re$\{E_r\}$ in ITER-FEAT.

the edge. The average energy of the beam ions in the core is 0.4 MeV, about one-third that of the fast alphas. The slowing down time for the beam ions in the centre is 1.15 s, longer than $\tau_{\rm slow}(0)$ of the fast alpha particles. This indicates that the NNBI could interfere with attempts to measure alpha parameters. An example of the distribution of the beam ions in energy and pitch angle at $x = 0.45$, averaged over the poloidal angle, is shown in figure 16.

The ICRH is assumed to be 53 MHz for He^3 resonance on-axis. The ICRH minority He^3 ions will not have high energy, and thus should not be a complication in studying fast alpha effects (and will not contribute significantly to stabilizing sawteeth or TAE). Their tail temperature, $T_{\rm min}(0)$ is close to $T_{\rm i}$, as shown in table 3.

The value of $\tau_{E,\rm th}$ is slightly below the $\tau_{\rm IPB98(y,2)}$ value. With the choice of a flat $n_{\rm e}$ profile, the form factor in equation (6) reduces $\tau_{E,\rm th}$ by a factor of 0.81. Since the profiles are held fixed during the flat-top phase as the heating power changes, the computed $\chi_{\rm eff}$ values change. The minimum

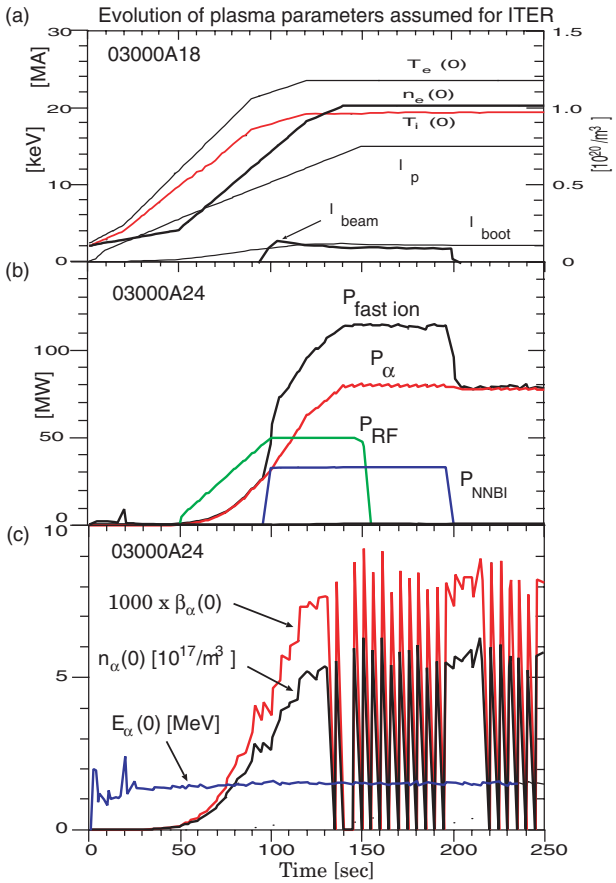

Figure 15. Time evolution of parameters in the ITER plasma. The alpha parameters in (c) are volume-averaged out to the $x = 0.1$ flux surface to reduce Monte Carlo fluctuations.

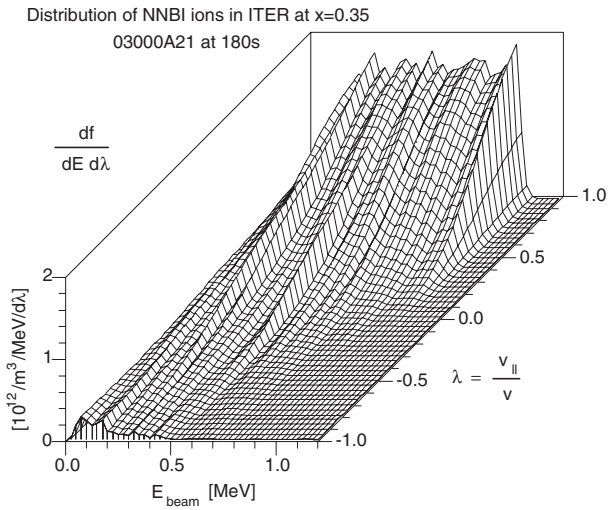

Figure 16. Distribution of the ITER NNBI beam ions in energy and pitch angle at $x = 0.35$, averaged over poloidal angle, computed by the TRANSP Monte Carlo model. The neutrals are injected at 1 MeV with $v_\parallel/v = 1$, and the beam ions become more isotropic as they slow down.

value during the phase of maximum heating (20 MW ICRH, 33 MW NNBI, and 75 MW alpha) is 0.7 [$m^2\,s^{-1}$]. The minimum drops to a more optimistic (i.e. harder to achieve) value of 0.5 [$m^2\,s^{-1}$] after the ICRH is shut off and later to

an even more optimistic 0.35 [$m^2\ s^{-1}$] after the NNBI is shut off. If χ_{eff} were held constant in time, the stored energy would change as the heating changed.

Alpha parameters have been calculated [28] for two ITER-EDA plasmas producing 1.5 GW fusion power. One had a nearly flat electron density profile, similar to the one used here for ITER-FEAT. The other had a relatively peaked n_e. The values for the alpha parameters calculated in the flat profile case are very similar to those given in table 5.

4. Summary and discussion

This paper reports results from TRANSP analysis of five plasmas with high DT fusion yield. The TFTR and JET plasmas with the highest values of P_{DT} obtained so far help to establish the scientific feasibility of energy production in future tokamak reactors. Three examples of plasmas from the proposed next step tokamaks with much higher P_{DT} are analysed. The plasma start-up and steady-state phases are modelled self-consistently, including auxiliary heating and accumulation of alpha ash. The results of this study include electronic files of the MHD equilibria, plasma parameters, and alpha parameters, and also distributions in energy and pitch angle and are available for use in studies of alpha effects and MHD and micro-turbulence instabilities.

The assumed plasma conditions for FIRE and ITER-FEAT are similar to examples proposed by their proponents. The assumed plasma conditions for IGNITOR differ in some inconsequential details from examples proposed by its proponents. These assumed plasma profiles and computed heat deposition profiles give values of $\tau_{E,th}$ close to the L-mode scaling in the case of IGNITOR and close to the ELMy H-mode fits in equations (5) and (6) in the cases of FIRE and ITER-FEAT.

Examples of results are the predictions (1) that if sawteeth occur in IGNITOR, they will not have adverse effects on the alpha parameters; (2) that pumping of the alpha ash will be needed in FIRE (and ofcourse in ITER) to maintain high P_{DT}; (3) that the He^3 minority ions will not be accelerated by ICRH to energies much above T_i in FIRE and ITER, and (4) that the NNBI ions will complicate measurement of fast alphas in ITER. The result (3) suggests that ICRH will not complicate measurements of fast alphas, and thus high fusion energy gain Q is not necessary for such measurements.

There are a number of interesting similarities and expected differences between the TFTR and JET plasmas and those considered for the next step burning plasma experiments in IGNITOR, FIRE, and ITER. Similarities include the values of $\beta_\alpha(0)$, $v_\alpha(0)/v_{Alfven}(0)$, and $\max\{-R \times \nabla(\beta_\alpha)\}$, which vary by a factor of at most four for the five plasmas. The value of $\max\{P_\alpha/P_{heat}\}$ varies by only a factor of 4.5. Steady-state profiles of the fast alpha density in IGNITOR, FIRE, and ITER-FEAT are expected to be very similar, as shown in figure 17. Steady-state profiles of $-R \times \nabla(\beta_\alpha)$ in IGNITOR, FIRE, and ITER-FEAT are shown in figure 18.

One major difference is that $T_i \gg T_e$ in the core of the TFTR and JET plasmas, whereas they are assumed and expected to be nearly equal in the next step tokamak plasmas since the energy equilibration should be fast at higher density. Another difference is that the TFTR and JET plasmas have

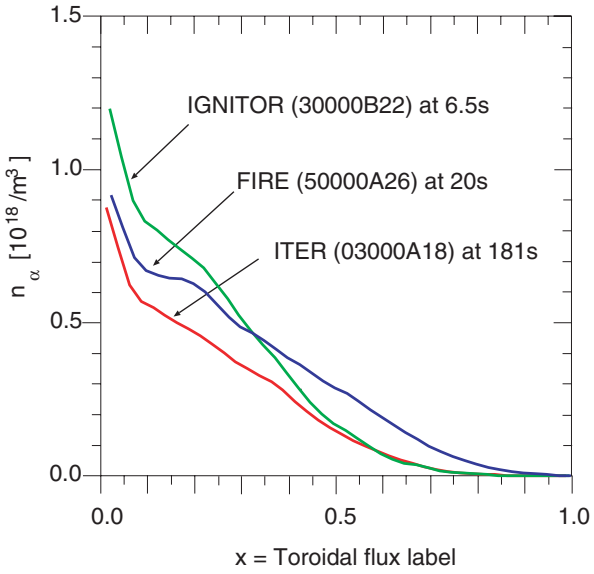

Figure 17. Profiles of the fast alpha densities in IGNITOR, FIRE, and ITER-FEAT during the steady-state phase.

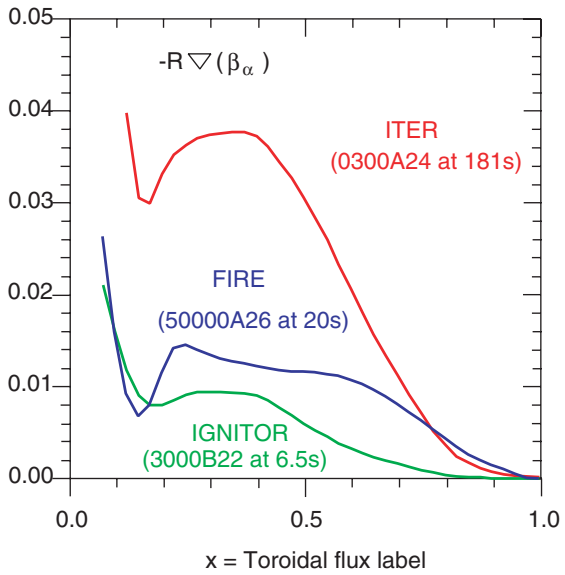

Figure 18. Profiles of $-R \times \nabla(\beta_\alpha)$ in IGNITOR, FIRE, and ITER-FEAT during the steady-state phase. The profiles have been smoothed, removing effects of sawteeth and Monte Carlo noise.

large toroidal rotation rates due to the intense NBI (with central Mach numbers of the carbon impurity being 0.25 and 1.6, respectively), whereas the next step plasmas are expected to have very low rotation rates due to the difficulty (cost) of injecting momentum into a tokamak reactor. Both $T_i \gg T_e$ and large rotation rates are correlated with high confinement in present-day experiments. Another difference is that the slowing down times for the alpha particles (τ_{slow}) is small compared to the thermal energy confinement times in the burning plasmas, unlike the situation in the achieved experiments.

Issues for future investigation include using models to predict the temperature profiles, and checking the MHD and micro-instability of the plasmas. Several predictive transport

models such as the multi-mode [29] and GLF23 [30] models have been incorporated into TRANSP, and could be used to predict the temperature profiles. The instability to ITG modes depends sensitively on the temperature gradients. If the plasmas are unstable, the pedestal temperatures may have to be increased to reduce the gradients while keeping the central values high enough for high $P_{\rm DT}$. However, it appears that the temperature at the separatrix should be well below 1 [keV] to prevent excessive sputtering erosion of surfaces down-stream in the divertor [31]. These constraints suggest the need for a large decrease in $T_{\rm i}$ between the top and bottom of the pedestal. Experiments in JET suggest that if there is in fact a large decrease in the pedestal, the ELMs would be Type I with excessive losses of energy in each ELM [32]. Gyrokinetic analysis of JET ELMy H-mode plasmas indicates that when the flow shear and linear micro-turbulence growth rates near the top of the pedestal are comparable, the energy confinement remains good [33]. This suggests that driving large flow shear near the top of the pedestal in next step tokamaks might permit high confinement and central temperatures with low pedestal temperatures.

Acknowledgments

This work was supported in part by the US DoE Contract No DE-AC02-76CH03073. The author wishes to thank the TRANSP development team for providing excellent analysis tools and the TFTR and JET teams for providing excellent plasmas.

References

[1] Angioni C. *et al* 2002 *Plasma Phys. Control. Fusion* **44** 205
[2] Porcelli F., Boucher D. and Rosenbluth M.N. 1996 *Plasma Phys. Control. Fusion* **38** 2163
[3] Fu G.F. *et al* 1996 *Phys. Plasmas* **3** 4036
[4] Budny R.V. *et al* 1995 *Nucl. Fusion* **35** 1497
[5] Fu G.Y., Chang C.Z. and Wong K.L. 1993 *Phys. Fluids* B **5** 4040
[6] Gorelenkov N., Chang C.Z. and Tang W.M. 1998 *Phys. Plasmas* **5** 3389
[7] Gorelenkov N. *et al* Study of thermonuclear Alfven instabilities in next step burning plasma proposals *Nucl. Fusion.* submitted
[8] Horton W. *et al* 2002 *Nucl. Fusion* **42** 169
[9] Airoldi A. and Cenacchi G. 2001 *Nucl. Fusion* **41** 687
[10] Coppi B. *et al* 2001 *Nucl. Fusion* **41** 1253
[11] Airoldi A. and Cenacchi G. 1997 *Nucl. Fusion* **37** 1117
[12] Meade D.M. *et al* 2001 *Proc. 18th Int. Conf. on Fusion Energy 2000 (Sorrento, 2000)* (Vienna: IAEA) CD-ROM file FTP2/16 and http://www.iaea.org/programmes/ripc/physics/fec2000/html/node1.htm
[13] Meade D.M. *et al* 2002 Exploration of burning plasmas in FIRE *Proc. 19th Int. Conf. on Fusion Energy 2002 (Lyon, 2002)* (Vienna: IAEA) submitted
[14] Campbell D.J. 2001 *Phys. Plasmas* **8** 2041
[15] Hawryluk R. 1998 *Rev. Mod. Phys.* **70** 537
[16] Keilhacker M. *et al* 1999 *Nucl. Fusion* **39** 209
[17] Goldston R.J. *et al* 1981 *J. Comput. Phys.* **43** 61
[18] Medley S.S. *et al* 1998 *Nucl. Fusion* **38** 1283
[19] McKee G.A., Fonck R.J., Stratton B.C., Budny R.V., Chang Z. and Ramsey A.T. 1997 *Nucl. Fusion* **37** 501
[20] Houlberg W., Shang K., Hirshman S. and Zarnstorff M. 1997 *Phys. Plasmas* **4** 3230
[21] Post D.E., Jensen R.V., Tarter C.B., Grasberger W.H. and Lokke W.A. 1977 *At. Data Nucl. Data Tables* **20** 397
[22] Sheffield J. 1985 *Tokamak Start-up* ed H. Knoepfel (New York: Plenum) p 11
[23] Evrard M., Ongena J. and van Eester D. 1995 Improved Dielectric Tensor in the ICRH module of TRANSP *AIP Conf. Proc. 335, Radio-Frequency Power in Plasmas, 11th Topical Conf. (Palm Springs, 1995)* p 235
[24] ITER Physics Basis 1999 *Nucl. Fusion* **39** 2137, see 2204–8
[25] Cordey J.G. *et al* 2001 *Proc. 28th EPS Conf. on Controlled Fusion and Plasma Physics (Madeira, Portugal)* vol 25A (ECA) P3.011, p 969
[26] Sharapov S.E. *et al* 1999 *Nucl. Fusion* **39** 373
[27] Jardin S.C., Pomphrey N. and Delucia J. 1986 *J. Comput. Phys.* **46** 481
[28] Budny R.V. *et al* 1996 *Phys. Plasmas* **3** 4583
[29] Bateman G., Kritz A.H., Kinsey J.E., Redd A.J. and Weiland J. 1998 *Phys. Plasmas* **5** 1793
[30] Waltz R.E. *et al* 1997 *Phys. Plasmas* **4** 2482
[31] Stangeby P.C. 2000 *The Plasma Boundary of Magnetic Fusion Devices* (Bristol and Philadelphia: Institute of Physics Publishing) p 232
[32] Loarte A. *et al* 2001 *Proc. 28th EPS Conf. (Madeira, 2001)* vol 25A (ECA) P3.005, p 945
[33] Budny R.V. *et al* 2002 *Nucl. Fusion* **42** 66